

Austenite Grain Growth Simulation in Welding Heat Affected Zone

Naoto FUJIYAMA*
Akira SEKI
Kazuhiro OGAWA

Toshinobu NISHIBATA
Hiroyuki HIRATA

Abstract

The pinning effect is useful for restraining austenite grain growth in low alloy steels and improving welding heat affected zone (HAZ) toughness in welded joints. We propose a new calculation model for predicting austenite grain growth behavior. The influence of grain boundary segregation on grain boundary mobility (solute-drag effect) is considered by multi-element systems and applied to an austenite grain growth simulation. Furthermore, calculation considering the temperature gradient in HAZ was performed. This calculation method provides a good analysis of the austenite grain growth behavior. We show the possibility of quantitatively predicting the effect of alloying elements and welding conditions.

1. Introduction

High heat input welding (e.g., submerged arc welding) is used for weld structures in the shipbuilding and construction sectors. In high heat input welding, the heat affected zone (HAZ) near the fusion line is heated to 1400°C or higher, which increases the size of prior austenite (γ) grains in the HAZ. This coarsens the fracture unit, which decreases the toughness.¹⁻³⁾ Some researchers have reported techniques that toughen HAZ using the pinning effect by non-metallic inclusion and intragranular transformation using oxides, as the nuclei of ferrite transformation are used.

For example, oxides such as TiO_2 ,⁴⁻⁶⁾ MnAl_2O_4 ,^{7,8)} Ti_2O_3 ,⁹⁾ Ti_2O_3 - TiN - MnS ,¹⁰⁻¹²⁾ Ti_2O_3 - MnS - BN ,¹³⁾ and TiN - MnS ¹⁴⁾ have been reported as intragranular ferrite nuclei. TiN ,¹⁵⁻¹⁸⁾ REM(O, S)-TiN ,¹⁹⁾ and oxides and sulfide including Mg and Ca²⁰⁾ have been reported as pinning particles. However, the optimum conditions of non-metallic inclusions, including their size and distribution that match the thickness, welding heat input, and required characteristics have not been clarified. In addition, various factors affect welds in a complicated manner, so it is experimentally difficult to extract and study each individual factor separately. Therefore, proposing a simulation method of welding microstructure—a model for predicting γ grain growth that is the basis of such simulation—is important.

Many studies have been conducted on the prediction of γ grain growth. Burke proposed the crystal grain growth formula (1).²¹⁾

$$R^n - R_0^n = kt \quad (1)$$

Where, R is the radius of the grain (m), t is time (s), k is the kinetic constant ($\text{m}^2 \cdot \text{s}^{-1}$), and n -value is selected from 2 to 4 based on the

rate-limiting steps. In addition, the grain growth is represented by the following kinetic formula for grain growth by the Gibbs-Thomson effect.

$$\frac{dR}{dt} = M^{\text{gb}} \times \frac{2\sigma V}{R} \quad (2)$$

Where, M^{gb} is the grain boundary mobility ($\text{m} \cdot \text{s}^{-1} \cdot \text{J}^{-1} \cdot \text{mol}$), σ is the grain boundary energy ($\text{J} \cdot \text{m}^{-2}$), and V is the molar volume ($\text{m}^3 \cdot \text{mol}^{-1}$). This formula represents the mobility and capillary effect and it can be replaced with Burke's formula. The solute-drag effect is an effective means of restraining γ grain growth in low-alloy steel. The solute-drag effect lowers the grain boundary mobility due to segregation of impurities as reported by Lücke and Detert,²²⁾ Cahn,²³⁾ Hillert and Sundman,²⁴⁾ Purdy and Brechet,²⁵⁾ and other researchers.

These researchers used numerical solution models to analyze the solute-drag effect and they mainly studied the effect in binary and ternary systems.²⁶⁻²⁸⁾ They have not studied how the solute-drag effect affects γ grain growth behavior. Formulae for predicting the pinning effect have been proposed in addition to those for the solute-drag effect. Zener proposed formula (3) showing the relationship between the diameter of a crystal grain and the radius of the particle (r (m)).²⁹⁾

$$R = \frac{4}{3} \frac{r}{f} \quad (3)$$

Where, f is the volume fraction of the pinning particle. Many formulae for predicting the pinning effect based on Zener's formula have been reported.³⁰⁻³⁵⁾

However, no researchers have studied how the pinning effect

* Researcher, Kimitsu R & D Lab.
1 Kimitsu, Kimitsu City, Chiba Pref. 299-1141

combined with the solute-drag effect affects γ grain growth behavior. In this study, a model for predicting the solute-drag effect in a multi-element system has been established and a formula for calculating γ grain growth considering the pinning effect is proposed. The formula was used to simulate γ grain growth in an isothermal process three-dimensionally. In addition, we have expanded the model to one considering the temperature gradient like HAZ on actual joints and used the model to simulate γ grain growth in HAZ two-dimensionally.

2. Experimental Procedures

Table 1 lists the chemical compositions of the sample steel. A vacuum melting furnace in the laboratory was used to make an ingot (100×180×200 mm). It was heated at 1150°C for two hours and then rolled to 20×200×1000 mm. The finishing temperature was 780°C. Water cooling began at 750°C and the cooling was stopped at 400°C.

Test pieces (11×11×60 mm) cut out from the rolled steel were tested in a reproduced heat cycle test. They were heated at 100°C/s, held at 1200°C and 1400°C for 1 to 30 seconds, and rapidly cooled with He gas. In addition, a groove was provided on the rolled steel plates and they were submerged arc welded at the heat input of 5.0 kJ/mm. After both tests, they were observed using an optical microscope to measure the size of prior γ grains.

3. Proposed Austenite Grain Growth Model³⁶⁾

3.1 Formula for γ grain growth considering the solute-drag effect

Figure 1 illustrates the movement of γ grain boundaries for pure iron (a) and when solute atoms are included (b).³⁷⁾ In this model, the liquid phase is a γ grain boundary phase and the numbers of atoms existing at the γ grain boundaries are supposed to be fixed. In Fig. 1 (a), when an iron atom enters the γ grain boundary, another iron atom existing at the γ grain boundary needs to move to the inside of the grain to keep the number of atoms at the boundary constant. The γ grain boundary moves as a result of such movement of iron atoms. This behavior can be expressed with formula (4).

$$v_{Fe} = I_{Fe} \cdot \delta \quad (4)$$

Where, v_{Fe} is the moving velocity of the iron atoms ($m \cdot s^{-1}$), I_{Fe} is the transition frequency (s^{-1}), and δ is the width of the grain boundary (m). In Fig. 1 (b), because solute atoms (i) exist, the concentration at the grain boundary is higher than that in the γ grain. This difference in the concentration decreases the γ grain boundary mobility. In a stationary state, the flux at which solute atoms (i) enter the γ grain boundary per unit time is equal to that of welding atoms (i) at the γ grain boundary, so formula (5) holds good.

$$\frac{X_i \times (\delta / \tau_i)}{V} = \frac{x_i \times v_{Fe}}{V} \quad (5)$$

Where, X_i is the atomic fraction of the atoms (i) at the γ grain boundary, τ_i is the time (s) during which the solute atoms (i) stay at the γ grain boundary, and x_i is the fraction of the solute atoms (i). Based on formula (5), the transition frequency (I_i) of the solute atoms (i) can be expressed with formula (6).

$$I_i = \frac{1}{\tau_i} = \frac{x_i}{X_i} \times \frac{v_{Fe}}{\delta} = \frac{x_i}{X_i} \times I_{Fe} \quad (6)$$

From formula (6), the moving velocity of the solute atoms (i) (v_i) can be expressed with formula (7).

$$v_i = I_i \cdot \delta = \frac{x_i}{X_i} \times I_{Fe} \cdot \delta \quad (7)$$

The force for developing crystal grains is the total of iron atoms and solute atoms (i) as shown with formula (8).

$$\Delta G = \frac{2\sigma V}{R} = \frac{X_{Fe}}{X_{Fe} + X_i} \times \frac{v}{M_{Fe}^{gb}} + \frac{X_i}{X_{Fe} + X_i} \times \frac{v}{M_i^{gb}} \quad (8)$$

Where, X_{Fe} is the fraction of Fe atoms at the γ grain boundary, M_{Fe}^{gb} is the pure iron's γ grain boundary mobility ($m \cdot s^{-1} \cdot J^{-1} \cdot mol$), and M_i^{gb} is the γ grain boundary mobility when the γ grain boundary is covered with solute atoms (i) in the Fe- i binary system ($m \cdot s^{-1} \cdot J^{-1} \cdot mol$). The total of the atomic fractions at the γ grain boundary is one, so formula (8) can be replaced with formula (9).

$$\frac{2\sigma V}{R} = \frac{v}{M_{Fe}^{gb}} \times (1 - X_i) + \frac{v}{M_i^{gb}} \times X_i = \left(\frac{1 - X_i}{M_{Fe}^{gb}} + \frac{X_i}{M_i^{gb}} \right) v \quad (9)$$

Therefore, formula (10) can be obtained.

$$\frac{dR}{dt} = v = \frac{1}{\frac{(1 - X_i)}{M_{Fe}^{gb}} + \frac{X_i}{M_i^{gb}}} \times \frac{2\sigma V}{R} \quad (10)$$

M_i^{gb} has a proportional relation with the transition frequency of pure iron and solute atoms (i), so formula (11) holds.

$$M_i^{gb} = \frac{x_i}{X_i} \times M_{Fe}^{gb} \quad (11)$$

From formulae (10) and (11), the speed of crystal grain growth in a binary system can be expressed with formula (12).

$$\frac{dR}{dt} = \frac{1}{(1 - X_i) + \frac{(X_i)^2}{x_i}} M_{Fe}^{gb} \times \frac{2\sigma V}{R} \quad (12)$$

When formula (12) is expanded to a multi-element system, the influence of each solute atom can be added as shown in formula (13).

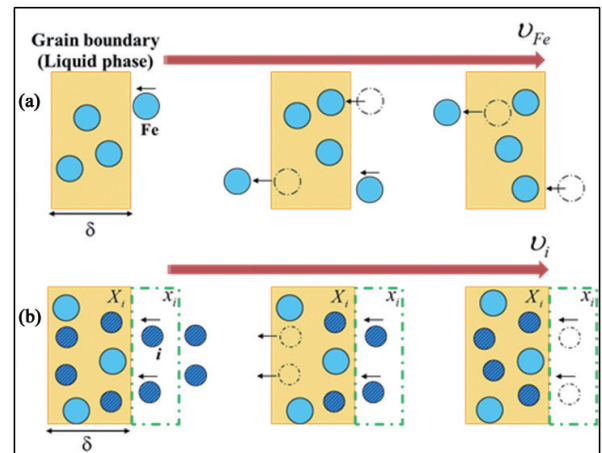


Fig. 1 Schematics of grain boundary movement³⁷⁾
(a) In pure iron and (b) Non-metallic including solute i

Table 1 Chemical compositions of the steels (mass%)

Heat	C	Si	Mn	P	S	Ti	Nb	Al	N	O
Steel A	0.05	0.14	1.60	0.01	0.002	—	0.006	0.02	0.0044	0.002
Steel B	0.05	0.14	1.60	0.01	0.002	0.012	0.006	0.02	0.0038	0.002

$$\frac{dR}{dt} = \frac{1}{\left(1 - \sum_{i \neq \text{Fe}} X_i\right) + \sum_{i \neq \text{Fe}} \frac{(X_i)^2}{x_i}} M_{\text{Fe}}^{\text{gb}} \times \frac{2\sigma V}{R} \quad (13)$$

Crystal grains grow and contract and adjacent crystal grains are linked at grain boundaries, so they are rather difficult to move compared to a single grain boundary. Therefore, by analyzing stable growth of the polycrystalline structure, formula (13) can be expressed as formula (14).³⁸⁾

$$\frac{dR}{dt} = \frac{1}{4} \frac{1}{\left(1 - \sum_{i \neq \text{Fe}} X_i\right) + \sum_{i \neq \text{Fe}} \frac{(X_i)^2}{x_i}} M_{\text{Fe}}^{\text{gb}} \times \frac{2\sigma V}{R} \quad (14)$$

3.2 Procedures for calculating the atomic fraction of atoms at γ grain boundaries

The fraction of the atoms (i) at the γ grain boundary needs to be calculated from formula (14). **Figure 2** illustrates mol free energy curves. $\mu_{\text{Fe}}^{\text{gb}}$ is the chemical potential of the pure iron at the γ grain boundary, μ_i^{gb} is the chemical potential of the solute atoms (i) at the γ grain boundary, μ_{Fe}^{γ} is the chemical potential of the pure iron in the γ phase, μ_i^{γ} is the chemical potential of the solute atoms (i) in the γ phase, G^{gb} is the mol free energy at the grain boundary, G^{γ} is the mol free energy in the γ phase, and x_i^{γ} is the fraction of the solute atoms (i) in the γ phase. In this model, the γ grain boundary is supposed to be a liquid phase and Hillert's law for parallel tangent lines was used.³⁹⁾ Therefore, the fraction of the atoms (i) at the γ grain

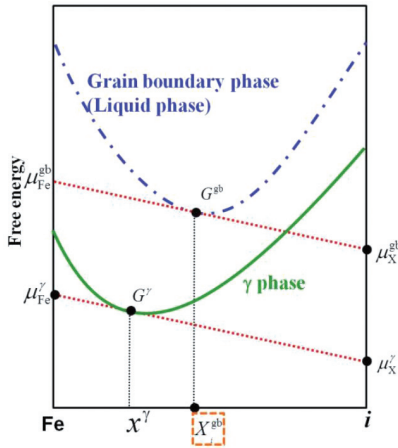


Fig. 2 Schematic diagram of free energy curves

boundary can be estimated from the grain boundary energy curve and the intersection point of the parallel tangent lines. Thermo-Calc was used for this calculation. The database was TCFE6. In addition, C, Si, Mn, P, S, and Nb were used as segregation elements for the calculation.

3.3 Calculation of γ grain growth using a phase-field model

A phase-field model⁴⁰⁻⁴²⁾ was used for two-dimensional calculation of γ grain growth simulating HAZ on actual joints. The phase-field equation is shown below.⁴²⁾

$$\frac{\partial \phi_i}{\partial t} = M^{\text{gb}} \sum_{j=1}^n \frac{1}{v} \left\{ \sum_{k=1}^n \left[(\sigma_{jk} - \sigma_{ik}) \left(\frac{\pi^2}{\delta^2} \phi_k + \nabla^2 \phi_k \right) \right] + \frac{2\pi}{\delta} \sqrt{\phi_i \phi_j} \Delta G_{ij} \right\} \quad (15)$$

Where, $\phi_{(i,j,k)}$ is a phase-field variable, v is 1 to 3 depending on the bulk and interface. σ_{jk} is the surface energy between crystal grains j and k , σ_{ik} is the interfacial energy between crystal grains i and k , δ is the width of the interface, and ΔG_{ij} is the force for developing crystal grains between i and j . In the phase-field model, each crystal grain is identified using a number and a phase-field variable is given. The growth of the crystal grains is calculated by solving the simultaneous equations.

In this calculation, MICRESS[®], a software for phase-field models, was used.⁴³⁾ In MICRESS[®], there is no need for input of a value to the grain boundary mobility. Therefore, formula (14) was used to calculate the γ grain boundary mobility in consideration of the solute-drag effect and the calculated value that was entered. As the σ value, the pure iron's grain boundary energy of 0.8 (J·mol⁻¹) was used. In MICRESS[®], a pinning effect can also be taken into account, so it was entered as the pinning force (κ) shown in formula (16).

$$\kappa = \frac{\Delta G_{\text{pin}}}{2\sigma V} \quad (16)$$

Where, ΔG_{pin} is the pinning energy (J·mol⁻¹). In this model, it was replaced as shown with formula (17) and calculated.^{29, 30)}

$$\Delta G_{\text{pin}} = \frac{3}{4} \frac{\sigma V f^{2/3}}{r} \quad (17)$$

Therefore, formula (16) will be formula (18). This formula was used for the calculation.

$$\kappa = \frac{3 f^{2/3}}{8r} \quad (18)$$

4. Simulation Results of γ Grain Growth

4.1 Study results of γ grain growth behavior in an isothermal process

Figure 3 shows the grain growth simulation results in an iso-

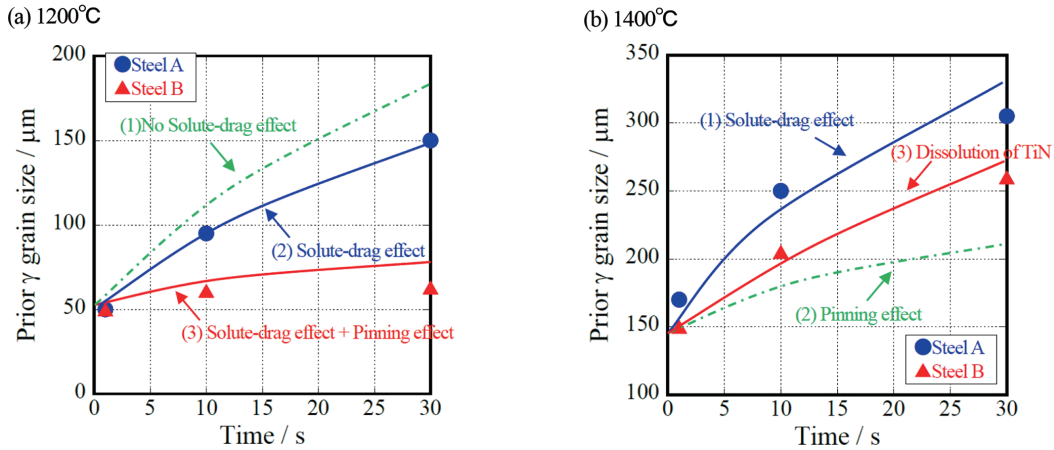


Fig. 3 Result of austenite grain growth simulation in an isothermal process

thermal process. Experimental results have been plotted in the graphs. Figure 3 (a) shows that for Steel A, when the solute-drag effect is not taken into account (1), there is no factor that restrains γ grain growth, so the calculated values are larger than the experimental values. On the other hand, when the solute-drag effect is taken into account (2), the calculated values almost match the experimental values. In addition, for Steel B, when the pinning effect is taken into account (3), the calculated values almost match the experimental values. TiN has been finely dispersed in Steel B and the volume fraction was calculated using Thermo-Calc. For the radius of TiN particles, 50 μm that was most often seen in the steel was substituted for calculation. As a result of the calculation at 1400°C of Fig. 3 (b), regarding Steel A, when the solute-drag effect is taken into account as well (1), the calculated values almost match the experimental values. These results show that it is important to consider the solute-drag effect for the γ grain boundary mobility to simulate actual γ grain growth behavior accurately.

On the other hand, regarding Steel B, when this model was used for calculation (2), the pinning effect worked too well and the calculated values were far from the experimental values. This is because TiN dissolved at approximately 1350°C, so the pinning effect decreased as time passed. Therefore, the dissolution formula⁴⁴⁾ shown as formula (19) was taken into account for calculation.

$$r^2 - r_0^2 = -2 \left(\frac{C_{\text{Ti(N)}}^{\gamma/\theta} - C_{\text{Ti(N)}}^0}{C_{\text{Ti(N)}}^{\theta} - C_{\text{Ti(N)}}^{\gamma/\theta}} \right) D_{\text{Ti(N)}}^{\gamma} \cdot t \quad (19)$$

Where, r_0 is the radius of the early TiN(θ) particles (m), $C_{\text{Ti(N)}}^{\gamma/\theta}$ is the Ti(N) concentration at the interface between the γ/θ phases, is the bulk Ti(N) concentration in the γ phase, $C_{\text{Ti(N)}}^0$ is the Ti(N) concentration in the θ phase, and $D_{\text{Ti(N)}}^{\gamma}$ is the volume diffusion coefficient of Ti(N) ($\text{m}^2 \cdot \text{s}^{-1}$). The formulae below were used for $D_{\text{Ti(N)}}^{\gamma}$.

$$D_{\text{Ti}}^{\gamma} = 1.5 \times 10^{-5} \exp\left(-\frac{251000}{RT}\right) \quad (20)$$

$$D_{\text{N}}^{\gamma} = 3.6 \times 10^{-5} \exp\left(-\frac{157000}{RT}\right) \quad (21)$$

In this calculation, local equilibrium at the interface was taken into account. In the calculation, it was assumed that the γ/θ interface of Ti was the same as that of N. Therefore, formula (22) holds good.

$$2 \left(\frac{C_{\text{Ti}}^{\gamma/\theta} - C_{\text{Ti}}^0}{C_{\text{Ti}}^{\theta} - C_{\text{Ti}}^{\gamma/\theta}} \right) D_{\text{Ti}}^{\gamma} \cdot t = 2 \left(\frac{C_{\text{N}}^{\gamma/\theta} - C_{\text{N}}^0}{C_{\text{N}}^{\theta} - C_{\text{N}}^{\gamma/\theta}} \right) D_{\text{N}}^{\gamma} \cdot t \quad (22)$$

This formula and solubility product of TiN were used to calculate $C_{\text{Ti(N)}}^{\gamma/\theta}$ and it was put into formula (19) to calculate the solubility. When dissolution is taken into account, the calculated values almost match the experimental values as shown as (3) in Fig. 3 (b).

The results above indicate that considering the solute-drag effect, pinning effect, and dissolution of non-metallic inclusion can make the simulation of γ grain growth behavior more accurate.

4.2 Simulation of γ grain growth in HAZ on welded joints

γ growth was calculated two-dimensionally simulating HAZ in consideration of a temperature gradient. Figure 4 shows the calculation conditions in MICRESS[®]. The calculation range was $500 \times 500 \mu\text{m}$. The grid size was $\Delta x = \Delta y = 1 \mu\text{m}$. The width of the interface was $6 \mu\text{m}$. The initial γ grain size was $35 \mu\text{m}$. In addition, the heat input of 5.0 kJ/mm was simulated. The fusion line section was set to 1400°C and the section 500 μm from the fusion line was set to 1200°C. Formula (14) was used to calculate the grain boundary mobility at each temperature. Figure 5 shows the calculation results. As the temperature is lower, the grain boundary mobility is lower so the solute-drag effect may be effective. Regarding the pinning ef-

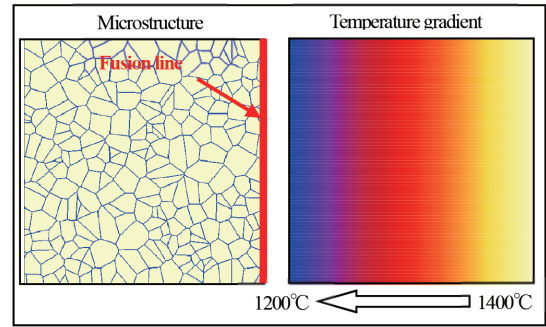


Fig. 4 Schematic of γ grain growth calculation condition in MICRESS[®]

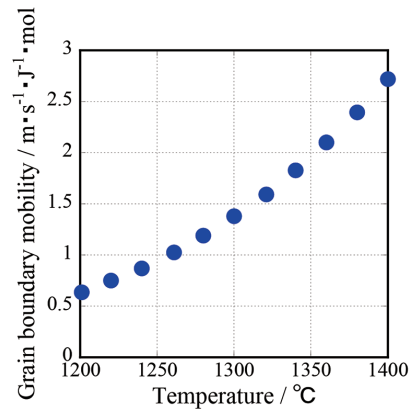


Fig. 5 Temperature dependency of γ grain boundary mobility

fect, the volume fraction was calculated using Thermo-Calc. The radius of TiN particles was calculated by substituting a value based on the reproduced heat cycle test results.

Figure 6 shows simulation results of γ grain growth in HAZ near the fusion lines. The figure shows that when only the solute-drag effect is taken into account (a), the size of the prior γ grains near the fusion line is the largest and it becomes smaller as the grains are farther away from the fusion line. However, since the pinning effect is not taken into account, the grains are generally coarser than those of the prior γ grain distribution at the actual weld (c). Meanwhile, when the solute-drag effect and pinning effects are taken into account (b), although the size of the prior γ grains near the fusion line is the largest and it becomes smaller as grains are further away from the fusion line as is the case when only the solute-drag effect is taken into account (a), the size of the prior γ grains is generally small due to the pinning effect. These simulation results almost match the prior γ grain distribution on the actual weld (c).

This calculation was two dimensional. The prior γ grain size distribution in the HAZ on actual joints can be reproduced at this level of the heat input. However, in simulation on the higher heat input side, the calculated values deviate from the experimental values. Some researchers have reported that there are differences between two-dimensional and three-dimensional calculation.⁴⁵⁾ Since this calculation was two-dimensional, the calculated values may differ. Expanding this phase-field model to three-dimensional calculation is our future task.

5. Conclusion

We proposed a new simulation model for predicting γ grain growth behavior. In this calculation model, the solute-drag effect in

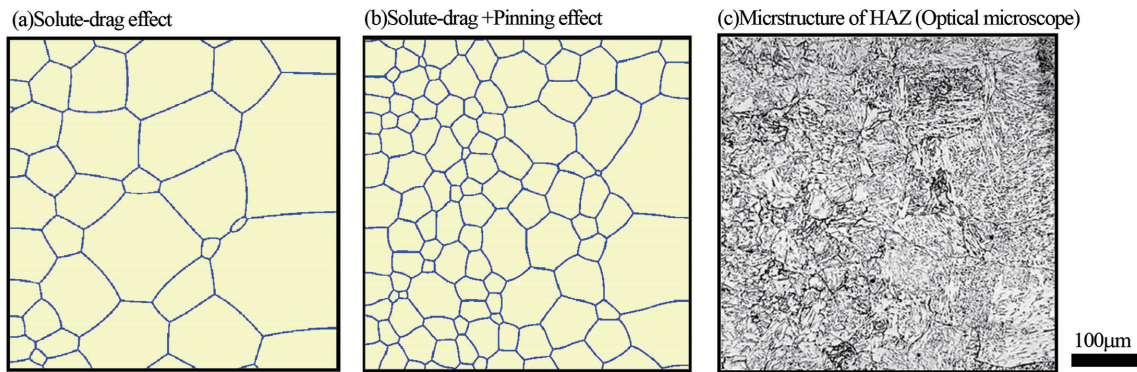


Fig. 6 Result of γ grain growth simulation at HAZ (5.0 kJ/mm)

a multi-element system was considered for γ grain boundary mobility and dissolution of non-metallic inclusion was considered for the pinning effect. In addition, a phase-field model was used for the simulation to visualize γ grain growth behavior. This model was used to simulate γ grain growth in an isothermal process and its appropriateness was checked. Furthermore, the model was expanded to one for which a temperature gradient was considered assuming HAZ on actual welds. As a result, the prior γ grain distribution in HAZ obtained by an experiment was accurately reproduced by γ grain growth simulation. These results show that the influence of alloying elements and welding conditions could be quantitatively predicted.

- 36) Fujiyama, N. et al.: Sci. Technol. Adv. Mater. 18, 88 (2017)
- 37) Nishizawa, T.: Mater. Trans. 42, 2027 (2001)
- 38) Hillert, M.: Acta Metall. 13, 227 (1965)
- 39) Hillert, M.: The Use of Gibbs Free Energy-Composition. In: Aaronson HI, Editor. Lectures on the Theory of Phase Transformations. Pennsylvania, The Metallurgical Society of AIME. 1975, p.36
- 40) Rabbe, D.: Computational Materials Science. Weinheim, Wiley-VCH, 1988
- 41) Steinbach, I. et al.: Physica D. 94, 135 (1996)
- 42) Eiken, J. et al.: Phys. Rev. E. 73, 066122-1 (2006)
- 43) MICRESS®: <http://www.micress.de> (accessed 2015-06-17)
- 44) Fujiyama, N. et al.: Preprints of the National Meeting of the Japan Welding Society. 93, 176 (2013)
- 45) Suwa, Y.: Nippon Steel Technical Report. 102, 19 (2013)

References

- 1) Cochrane, R. C.: Welding in the World. 21, 16 (1983)
- 2) Tweed, J. H., Knott J. F.: Acta Metall. 35, 1401 (1987)
- 3) Ameyama, K. et al.: Tetsu-to-Hagané. 74, 1839 (1988)
- 4) Mori, N. et al.: J. Jpn. Weld. Soc. 50, 786 (1981)
- 5) Watanabe, I. et al.: J. Jpn. Weld. Soc. 52, 773 (1980)
- 6) Mills, A. R. et al.: Mater. Sci. Technol. 3, 1051 (1987)
- 7) Thewlis, G.: Mater. Sci. Technol. 10, 110 (1994)
- 8) Grong, Ø. et al.: Metall. Trans. A. 26A, 525 (1995)
- 9) Byun, J. S. et al.: Mater. Sci. Eng A. 319-321, 326 (2001)
- 10) Imaginbai, M. et al.: HSLA Steels'85. 1985, p. 557
- 11) Chijiwa, R. et al.: Proceeding of the 7th Int. Conf. OMAE, Houston, ASME. 1988, p. 165
- 12) Yamamoto, K. et al.: Residual and Unspecified Elements in Steels. AS-TEM STP1042. 1989, p. 266
- 13) Yamamoto, K. et al.: Tetsu-to-Hagané. 79, 1169 (1993)
- 14) Tomita, Y. et al.: ISIJ International. 34, 829 (1994)
- 15) Kanazawa, S. et al.: Tetsu-to-Hagané. 61, 2589 (1975)
- 16) Nakanishi, M. et al.: Q. J. Jpn. Weld. Soc. 52, 117 (1983)
- 17) Kasamatsu, Y. et al.: Tetsu-to-Hagané. 65, 1232 (1979)
- 18) Rak, I. et al.: Metall. Mater. Trans. A. 28A, 199 (1997)
- 19) Deshimaru, S. et al.: Kawasaki Steel Technical Report. 18, 295 (1996)
- 20) Kojima, A. et al.: Nippon Steel Technical Report. 90, 1 (2004)
- 21) Burke, J. E., Turnbull, D.: Recrystallization and Grain Growth, Progress in Physics 3. Ed. B. Chalmers, London, Pergamon Press, 1952, p. 220
- 22) Lücke, K., Detert, K.: Acta Met. 5, 628 (1957)
- 23) Cahn, J. W.: Acta Met. 10, 789 (1962)
- 24) Hillert, M., Sundman, B.: Acta Met. 24, 731 (1976)
- 25) Purdy, G. R., Brechet, Y. J. M.: Acta Met. 43, 3763 (1995)
- 26) Turnbull, D.: Trans. ASME. 191, 661 (1951)
- 27) Nishizawa, T.: Tetsu-to-Hagané. 70, 1984 (1984)
- 28) Hillert, M.: Institute of Metals. 231 (1968)
- 29) Zener, C. Quoted by Smith, S.: Trans. AIME. 175, 15 (1948)
- 30) Nishizawa, T. et al.: Mat Trans. JIM. 38, 950 (1997)
- 31) Gladman, T.: Proc. Roy. Soc. A294, 298 (1966)
- 32) Hillert, M.: Acta Metall. 36, 3177 (1988)
- 33) Hunderi, O., Ryum, N.: Acta Metall. Mater. 40, 543 (1992)
- 34) Srolovitz, D. J. et al.: Acta Metall. 32, 1429 (1984)
- 35) Anderson, M. P. et al.: Scripta Metall. 23, 753 (1989)



Naoto FUJIYAMA
Researcher
Kimitsu R & D Lab.
1 Kimitsu, Kimitsu City, Chiba Pref. 299-1141



Toshinobu NISHIBATA
Senior Researcher
Fundamental Metallurgy Research Lab.
Advanced Technology Research Laboratories



Akira SEKI
Specialized Senior Manager, Dr. Eng.
Numerical Analysis Solution Div.
Nippon Steel & Sumikin Technology Co., Ltd.



Hiroyuki HIRATA
General Manager, Head of Lab., Ph.D
Welding & Joining Research Lab.
Steel Research Laboratories



Kazuhiro OGAWA
Ph.D
Researcher delegated by Nippon Steel & Sumitomo
Metal Corporation